Available online at www.sciencedirect.com
SCIENCE DIRECT®
International Journal of Thermal Sciences 43 (2004) 979–991
International Journal of Thermal Sciences
www.elsevier.com/locate/ijts

Numerical simulation of triple concentric-tube heat exchangers

O. García-Valladares

Centro de Investigación en Energía (CIE), Universidad Nacional Autónoma de México (UNAM), Privada Xochicalco S/N, Temixco, 62580 Morelos, Mexico

Received 12 August 2003; received in revised form 30 January 2004; accepted 16 February 2004

Available online 21 April 2004

Abstract

A detailed one-dimensional steady and transient numerical simulation of the thermal and fluid-dynamic behaviour of triple concentric-tube heat exchangers has been developed. The governing equations (continuity, momentum and energy) inside the inner tube and the annulus (inner and outer), together with the energy equations in the inner, intermediate and outermost tube wall and insulation, are solved iteratively in a segregated manner. The discretized governing equations in the zones with fluid flow are coupled using an implicit step by step method. This formulation requires the use of empirical information for the evaluation of convective heat transfer, shear stress and void fraction. An implicit central difference numerical scheme and a line-by-line solver was used in the inner and intermediate tube walls and the outermost tube wall with insulation. All the flow variables (enthalpies, temperatures, pressures, mass fractions, velocities, heat fluxes, etc.) together with the thermophysical properties are evaluated at each point of the grid in which the domain is discretized. Different numerical aspects and comparisons with results obtained from the technical literature are presented in order to verify and validate the model.

Keywords: Heat exchanger; Triple-tube; Concentric; Numerical simulation; Pasteurizers

1. Introduction

Triple concentric-tube heat exchangers are used for different products and are found in dairy, food, beverage and pharmaceutical industries. Almost all liquid products can be pasteurized through one of these heat exchangers. Examples of such products are milk, cream, pulpy orange juice, apple mash, liquid eggs, sauces, etc.

Triple concentric-tube heat exchangers improve the heat transfer through an additional flow passage and a larger heat transfer area per unit exchanger length compared to a double concentric-tube heat exchanger.

In order to optimise the effectiveness of the heat exchangers, and consequently the energy consumption and cost, more accurate and general methods of prediction of their thermal and fluid-dynamic behaviour are required. The inherent complexity of the heat exchanger design in aspects such as geometries and fluid flow patterns, means that the possibilities of analytical solutions are very limited without assuming stringent simplifications (e.g., analytical approaches such as F-factor, ε-NTU, etc.). Numerical methods allow the governing equations to be solved with fewer restrictions.

An important variety of technical situations can be treated assuming steady or transient one-dimensional flow, for example, all those involving flow through tubes and ducts (double pipe, shell-and-tube, fin-and-tube heat exchangers, etc.).

Zuritz [1] developed a set of analytical equations for fluid temperatures and conducted a case study for triple tube counter-flow heat exchanger. Ünal [2] obtained a fully analytical expressions for the variations of bulk temperatures of the three fluid streams along the heat exchanger based on a simplified physical model. Ünal [3] presented several case studies for counter-flow arrangement and it has been demonstrated that the heat exchanger performance/or size is strongly dependent upon the radii of the three tubes. Ünal [4] derived a fully analytical expressions for the effectiveness of triple concentric-tube heat exchangers with both counter-flow and parallel-flow arrangements based on the previously obtained temperature distribution expressions [2].

The objective of this work is to develop numerical criteria which allow the simulation, in both transient and steady state, of the thermal and fluid-dynamic behaviour of a triple concentric-tube heat exchanger. The numerical solution in the zones with fluid flow has been performed by discretization of the one-dimensional governing equations

E-mail address: ogv@cie.unam.mx (O. García-Valladares).

1290-0729/$ – see front matter
doi:10.1016/j.ijthermalsci.2004.02.006

Nomenclature

A	cross section area	m^2
c_p	specific heat at constant pressure	$J{\cdot}kg^{-1}{\cdot}K^{-1}$
CV	control volume	
D	diameter	m
e	specific energy ($h + v^2/2 + gz\sin\theta$)	$J{\cdot}kg^{-1}$
f	friction factor	
g	acceleration due to gravity	$m{\cdot}s^{-2}$
G	mass velocity	$kg{\cdot}m^{-2}{\cdot}s^{-1}$
h	enthalpy	$J{\cdot}kg^{-1}$
L	length	m
m	mass	kg
$\dot{m}$	mass flux	$kg{\cdot}s^{-1}$
n	number of control volumes	
p	pressure	Pa
P	perimeter	m
P_T	friction power expenditure	W
$\dot{q}$	heat flux per unit area	$W{\cdot}m^{-2}$
$\dot{Q}$	heat flux	W
r	radius	m
Re	Reynolds number ($\frac{GD}{\mu}$)	
t	time	s
T	temperature	K
v	velocity	$m{\cdot}s^{-1}$
x_g	vapour mass fraction	
z	axial coordinate	

Greek letters

θ	angle	rad
ρ	density	$kg{\cdot}m^{-3}$
Φ	two-phase frictional multiplier	
α	heat transfer coefficient	$W{\cdot}m^{-2}{\cdot}K^{-1}$
δ	rate of convergence	
ξ	roughness	m
τ	shear stress	Pa
λ	thermal conductivity	$W{\cdot}m^{-1}{\cdot}K^{-1}$
μ	dynamic viscosity	Pa·s
ε	effectiveness of the heat exchanger	
ε_g	void fraction	
Δp	pressure drop	Pa
Δt	temporal discretization step	s
Δr	radial discretization step	m
Δz	axial discretization step	m

Subscripts

E, e	east
g	gas or vapour
inner	annulus inner surface
l	liquid
N, n	north
outer	annulus outer surface
r	radial direction
S, s	south
tp	two-phase
W, w	west
z	axial direction
o	previous instant

Superscripts

$*$	guessed values
$-$	arithmetical average over a CV: $\bar{\phi} = (\phi_i + \phi_{i+1})/2$
$\sim$	integral average over a CV: $\tilde{\phi} = (1/\Delta z)\int_z^{z+\Delta z} \phi \, dz$

based on an efficiently coupled fully implicit step by step method over control volumes (CVs) [5–7].

The local fluids products and water thermophysical properties are evaluated using values obtained from technical literature and REFPROP v.7.0 [8], respectively. The solid elements (tubes and insulation) are accurately solved considering multidimensional heat transfer effects.

Details of the mathematical formulation and the different numerical techniques employed are firstly shown. Then, different numerical aspects are presented and finally comparisons of numerical solutions with results obtained in the literature are shown.

2. Mathematical formulation

2.1. Flow inside ducts

The mathematical formulation of the two-phase flow is evaluated inside a characteristic CV of a tube (single-phase flow, liquid or gas, represents a particular case). A characteristic CV is shown schematically in Fig. 1, where 'i' and '$i+1$' represent the inlet and outlet sections respectively.

Taking into account the characteristic geometry of ducts (diameter or diameters, length, roughness, angle, etc.), the

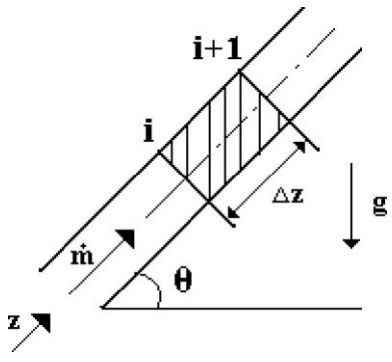

Fig. 1. Flow inside a control volume.

governing equations have been integrated assuming the following assumptions:

- one-dimensional flow: $p(z,t)$, $h(z,t)$, $T(z,t)$, etc.
- negligible axial heat conduction inside the fluid and radiation effects.

The semi-integrated governing equations over the above mentioned finite CV, have the following form [7]:

- Continuity:

$$\left[\dot{m}\right]_i^{i+1} + \frac{\partial m}{\partial t} = 0 \tag{1}$$

- Momentum:

$$\left[\dot{m}_g v_g\right]_i^{i+1} + \left[\dot{m}_l v_l\right]_i^{i+1} + \Delta z \frac{\partial \tilde{\dot{m}}}{\partial t} = -[p]_i^{i+1} A - \tilde{\tau} P \Delta z - \text{mgsin}\,\theta \tag{2}$$

- Energy:

$$\tilde{m}[e_l]_i^{i+1} + \left[\dot{m}_g(e_g - e_l)\right]_i^{i+1} + \left(\tilde{e}_g - \tilde{e}_l\right)\frac{\partial m_g}{\partial t} + m_g \frac{\partial \tilde{e}_g}{\partial t} + m_l \frac{\partial \tilde{e}_l}{\partial t} - A\Delta z \frac{\partial \tilde{p}}{\partial t} + \left(\tilde{e}_l - \bar{e}_l\right)\frac{\partial m}{\partial t} = \tilde{\dot{q}} P \Delta z \tag{3}$$

where $\tilde{\phi}$ represents the integral volume average of a generic variable ϕ over the CV and $\bar{\phi}$ its arithmetic average between the inlet and outlet of the CV. The subscript and superscript in the brackets indicate $[X]_i^{i+1} = X_{i+1} - X_i$, i.e., the difference between the quantity X at the outlet section and the inlet section.

In the governing equations, the evaluation of the shear stress is performed by means of friction factor f. This factor is defined from the expression: $\tau = \Phi(f/4)(G^2/2\rho)$ [9], where Φ is the two-phase factor multiplier. The one-dimensional model also requires the knowledge of the two-phase flow structure, which is evaluated by means of the void fraction ε_g. Finally, heat transfer through the duct wall and fluid temperature are related by the convective heat transfer coefficient α, which is defined as: $\alpha = \dot{q}_{\text{wall}}/(T_{\text{wall}} - T_{\text{fluid}})$.

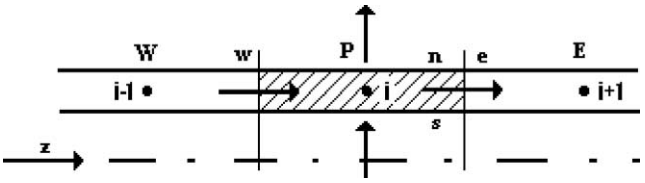

Fig. 2. Heat fluxes in a control volume of a solid.

2.2. Heat conduction in the inner and intermediate tubes wall

The conduction equation has been written assuming the following hypotheses: one-dimensional transient temperature distribution and negligible heat exchanged by radiation. A characteristic CV is shown in Fig. 2, where 'P' represents the central node, 'E' and 'W' indicate its neighbours. The CV-faces are indicated by 'e', 'w', 'n' and 's'.

Integrating the energy equation over this CV, the following equation is obtained:

$$\left(\tilde{\dot{q}}_s P_s - \tilde{\dot{q}}_n P_n\right)\Delta z + \left(\tilde{\dot{q}}_w - \tilde{\dot{q}}_e\right)A = m\frac{\partial \tilde{h}}{\partial t} \tag{4}$$

where $\tilde{\dot{q}}_s$ and $\tilde{\dot{q}}_n$ are evaluated using the respective convective heat transfer coefficient in each zone, and the conductive heat fluxes are evaluated from the Fourier law, that is: $\tilde{\dot{q}}_e = -\lambda_e(\partial T/\partial z)_e$ and $\tilde{\dot{q}}_w = -\lambda_w(\partial T/\partial z)_w$.

2.3. Heat conduction in the outermost tube wall and the insulation

The outermost tube wall is solved in a similar way as described in the previous section for the inner and intermediate tubes. The conduction equation for the insulation has been written assuming transient axisymmetric temperature distribution and negligible heat exchange by radiation with the external ambient. Eq. (4) can also be applied over the annular CVs in the insulation (see Fig. 3). The north and south interfaces are evaluated from the Fourier law, except in the tube-insulation interface (where a harmonic mean is used taking into account the distances between the interface

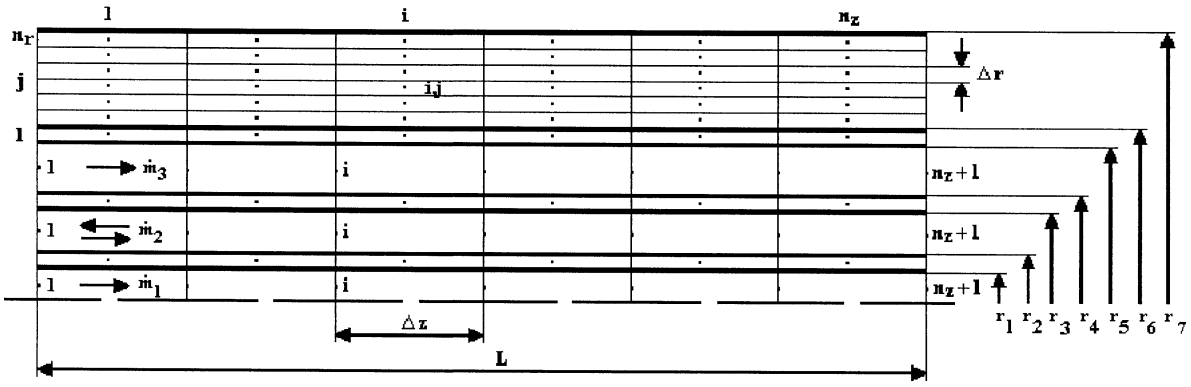

Fig. 3. Node distribution along the triple concentric-tube heat exchanger.

and the central node of the CV in the interface in both materials together with their different conductivities) and in the insulation-ambient interface where the heat transfer by natural convection is introduced.

3. Differentiation between Regions (if change of phase, condensation or evaporation, occurs)

The differentiation between the three main regions existing in both the condensation and the evaporation processes is given by the enthalpy, pressure and vapour quality. These conditions are:

- Liquid region: when $h(p) < h_l(p)$, then $x_g = 0$.
- Two-phase region: when $h_l(p) \leqslant h(p) \leqslant h_g(p)$, then $0 < x_g < 1$.
- Vapour region: when $h(p) > h_g(p)$, then $x_g = 1$.

Where $h_l(p)$ and $h_g(p)$ represent the saturation liquid and gas enthalpy for a given pressure p.

4. Evaluation of empirical coefficients

The mathematical model requires information about friction factor f, convective heat transfer coefficient α and the void fraction ε_g. This information is generally obtained from empirical or semi-empirical correlations. After comparing different empirical correlations presented in the technical literature, the following one was selected for in this article:

Single-phase

In the *single-phase regions* (subcooled liquid or superheated vapour), the convective heat transfer coefficient is calculated using the Nusselt number for uniform heat flux and the Gnielinski equations [10] for laminar and turbulent regimes respectively (the change between both regimes is considered when the Reynolds number is equal to 2000). The friction factor is evaluated from the expressions proposed by Churchill (cited by Lin et al. [11]). The void fraction and mass fraction (quality) is equal to 1 if the fluid is a superheated vapour and zero if it is a subcooled liquid.

Annulus flow

The friction factor is calculated using the expressions corresponding to single-phase flow with the hydraulic diameter. For turbulent regimes, the convective heat transfer due to both tube walls are calculated using the Monrad and Pelton correlations proposed specifically for annulus (cited by Jakob [12]); for laminar ones, Martin [13] correlation for annulus with both surfaces heated is used.

5. Numerical resolution

5.1. Spatial and temporal discretization

Fig. 3 shows the spatial discretization of a triple concentric-tube heat exchanger. The discretization nodes are located at the inlet and outlet sections of the CVs in the fluid flow zones, while the discretization nodes are centred in the CVs in the tubes wall and insulation. Each one of the fluids has been divided into n_z volumes (i.e., $n_z + 1$ nodes). The internal tubes has been discretized into n_z control volumes of length Δz. The external tube and the insulation are discretized into $n_z x n_r$ control volumes of length Δz and width Δr, where $\Delta r = (r_6 - r_5)$ for $j = 1$ and $\Delta r = (r_7 - r_6)/(n_r - 1)$ for $j > 1$.

The transitory solution is performed at every time step Δt. Depending on the time evolution of the boundary conditions, a constant or variable value of Δt can be selected.

5.2. Flow inside annulus and the inner tube

The discretized equations have been coupled using a fully implicit step by step method in the flow direction. From the known values at the inlet section (pressure and temperature or quality) and guessed values of the wall boundary conditions (wall temperature distribution obtained from the previous outer iteration), the variable values at the outlet of each CV are iteratively obtained from the discretized governing equations (see next section). This solution (outlet values) is the inlet values for the next CV. The procedure is carried out until the end of the tube is reached.

5.2.1. Discretization equations

For each CV, a set of algebraic equations is obtained by a discretization of the governing equations (1)–(3).

In the section *mathematical formulation*, the governing equations have been directly presented on the basis of the spatial integration over finite CVs. Thus, only their temporal integration is required. The transient terms of the governing equations are discretized using the following approximation: $\partial\phi/\partial T \cong (\phi - \phi^o)/\Delta t$, where ϕ represents a generic dependent variable ($\phi = h,\ p,\ T,\ \rho$, etc.); superscript "o" indicates the value of the previous instant.

The integral volume averages of the different variables have been estimated by the arithmetic mean between their values at the inlet and outlet sections, that is: $\tilde{\phi}_i \cong \bar{\phi}_i \equiv (\phi_i + \phi_{i+1})/2$.

Based on the numerical approaches indicated above, the governing equations (1)–(3) can be discretized to obtain the value of the dependent variables (mass flow rate, pressure and enthalpy) at the outlet section of each CV. The final form of the governing equations are given below.

The mass flow rate is obtained from the discretized *continuity equation*,

$$\dot{m}_{i+1} = \dot{m}_i - \frac{A\Delta z}{\Delta t}\left(\bar{\rho}_{\text{tp}} - \bar{\rho}^o_{\text{tp}}\right) \tag{5}$$

where the two-phase density is obtained from: $\rho_{\text{tp}} = \rho_g \varepsilon_g + (1-\varepsilon_g)\rho_l$.

In terms of the mass flow rate, gas and liquid velocities are calculated as,

$$v_g = \left[\frac{\dot{m}x_g}{\rho_g \varepsilon_g A}\right], \qquad v_l = \left[\frac{\dot{m}(1-x_g)}{\rho_l(1-\varepsilon_g)A}\right]$$

The discretized *momentum equation* is solved for the outlet pressure,

$$\begin{aligned} p_{i+1} = p_i - \frac{\Delta z}{A}\Bigg[&\left(\Phi_{\text{inner}}\bar{f}_{\text{inner}}P_{\text{inner}} + \Phi_{\text{outer}}\bar{f}_{\text{outer}}P_{\text{outer}}\right) \\ &\times \frac{\bar{\dot{m}}^2}{8\bar{\rho}_{\text{tp}}A^2} + \bar{\rho}_{\text{tp}}\,\text{Ag}\sin\theta \\ &+ \frac{[\dot{m}(x_g v_g + (1-x_g)v_l)]_i^{i+1}}{\Delta z} + \frac{\bar{\dot{m}} - \bar{\dot{m}}^o}{\Delta t}\Bigg] \end{aligned} \tag{6}$$

where, the subscript 'inner' and 'outer' in the annulus indicates the effects of friction due to the inner and outer surfaces. In the case of the flow in the inner tube only the outer surface exists.

From the *energy equation* (3) and the *continuity equation* (1), the following equation is obtained for the outlet enthalpy:

$$\begin{aligned} h_{i+1} = \Bigg[&2\left(\dot{q}_{\text{wall,inner}}P_{\text{inner}} + \dot{q}_{\text{wall,outer}}P_{\text{outer}}\right)\Delta z \\ &- \dot{m}_{i+1}a + \dot{m}_i b + \frac{A\Delta z}{\Delta t}c\Bigg] \\ &\times \left[\dot{m}_{i+1} + \dot{m}_i + \frac{\bar{\rho}^o_{\text{tp}}A\Delta z}{\Delta t}\right]^{-1} \end{aligned} \tag{7}$$

where

$$a = \left(x_g v_g + (1-x_g)v_l\right)^2_{i+1} + g\sin\theta\Delta z - h_i$$

$$b = \left(x_g v_g + (1-x_g)v_l\right)^2_{i} - g\sin\theta\Delta z + h_i$$

$$c = 2\left(\bar{p}_i - \bar{p}^o_i\right) - \bar{\rho}^o_{\text{tp}}\left(h_i - 2\bar{h}^o_i\right) - \left(\bar{\rho}\bar{v}_i^2 - \bar{\rho}^o\bar{v}_i^{o^2}\right)$$

Temperature, mass fraction and thermophysical properties are evaluated using matrix functions of the pressure and enthalpy, refilled with the fluid products properties evaluated using literature information or REFPROP v.7.0 (in the case of water and air) [8]:

$$T = f(p,h), \qquad x_g = f(p,h), \qquad \rho = f(p,h), \ldots \tag{8}$$

The above mentioned conservation equations of mass, momentum and energy together with the thermophysical properties, are applicable to transient two-phase flow. Situations of steady flow and/or single-phase flow (liquid or gas) are particular cases of this formulation. Moreover, the mathematical formulation in terms of enthalpy gives generality of the analysis (only one equation is needed for all the regions) and allows to deal with cases of mixtures of fluids.

5.2.2. Boundary conditions

Inlet conditions. The boundary conditions for solving a step by step method directly are the inlet mass flux ($\dot{m}_{\text{in}}$), pressure (p_{in}) and temperature (T_{in}) or mass fraction (x_{gin}) in the cases of two-phase flow. From any of these values (temperature or mass fraction) and the pressure, enthalpy (the dependent variable) is obtained. Other boundary conditions such as ($\dot{m}_{\text{in}}$, p_{out}) or (p_{in}, p_{out}) or (p_{in}, $\dot{m}_{\text{out}}$) can be solved using a Newton–Raphson algorithm. The method is based on an iterative process where the inlet mass flux or the inlet pressure is updated until global convergence is reached.

Solid boundaries. The wall temperature profile in the tube (constant or variable) or the heat flux through the tube wall in each CV must be given. These boundary conditions are expressed in the energy equation in the following compact form:

$$\dot{q}_{\text{wall}} = (1-\beta)\dot{q}_{\text{wall}} + \beta\alpha(T_{\text{wall}} - T_{\text{fluid}}) \tag{9}$$

where $\beta = 1$, if the boundary condition is the wall temperature, and $\beta = 0$, if the heat flux is given. An adiabatic boundary condition can be given if $\beta = 0$ and $\dot{q}_{\text{wall}} = 0$.

5.2.3. Solver

In each CV, the values of the flow variables at the outlet section of each CV are obtained by solving iteratively the resulting set of algebraic equations (continuity, momentum, energy and state equations mentioned above) from the known values at the inlet section and the boundary conditions. The solution procedure is carried out in this manner, moving forward step by step in the flow direction. At each cross section, the shear stresses, the convective heat fluxes and the void fractions are evaluated using the empirical correlations obtained from the available literature (see *Evaluation of Empirical Coefficients*). The transitory solution is iteratively performed at each time step. Depending on the time evolution of the boundary conditions, a constant or variable value of Δt can be selected.

5.2.4. Convergence

Convergence is verified at each CV using the following condition:

$$\left(1 - \left|\frac{\phi^*_{i+1} - \phi_i}{\Delta\phi}\right|\right) < \delta \tag{10}$$

where ϕ refers to the dependent variables of mass flux, pressure and enthalpy; and ϕ^* represents their values at the previous iteration. The reference value $\Delta\phi$ is locally evaluated as $\phi_{i+1} - \phi_i$. When this value ($\Delta\phi$) tends to be zero, for example, in the case of mass flux variable in steady state ($\dot{m}_{i+1} = \dot{m}_i$), $\Delta\phi$ is substituted by ϕ_{i+1} and the numerator is substitued by ϕ^*_{i+1}.

5.3. Heat conduction in the inner and intermediate tube wall

The following equation has been obtained from Eq. (4) for each node of the grid:

$$a_i T_{\text{wall},i} = b_i T_{\text{wall},i+1} + c_i T_{\text{wall},i-1} + d_i \tag{11}$$

where the coefficients are,

$$a_i = \frac{\lambda_w A}{\Delta z} + \frac{\lambda_e A}{\Delta z} + (\alpha_s P_s + \alpha_n P_n)\Delta z + \frac{A\Delta z}{\Delta t}\rho c_p$$

$$b_i = \frac{\lambda_e A}{\Delta z}$$

$$c_i = \frac{\lambda_w A}{\Delta z}$$

$$d_i = \left(\alpha_s P_s \overline{T}_s + \alpha_n P_n \overline{T}_n\right)\Delta z + \frac{A\Delta z}{\Delta t}\rho c_p T^o_{\text{wall},i}$$

The coefficients mentioned above are applicable for $2 \leqslant i \leqslant n_z - 1$; for $i = 1$ and $i = n_z$ appropriate coefficients are used to take into account the axial heat conduction or temperature boundary conditions. The set of heat conduction discretized equations is solved using the algorithm TDMA [14].

5.4. Heat conduction in the outermost tube and insulation

The following equation has been obtained for each node of the grid:

$$a_P T_{\text{wall},i,j} = a_E T_{\text{wall},i+1,j} + a_W T_{\text{wall},i-1,j} + a_N T_{\text{wall},i,j+1} + a_S T_{\text{wall},i,j-1} + d_P \tag{12}$$

where the coefficients are,

$$a_W = \frac{\lambda_w A}{\Delta z}, \qquad a_E = \frac{\lambda_e A}{\Delta z}, \qquad a_N = \frac{\lambda_n P_n \Delta z}{\Delta r}$$

$$a_S = \frac{\lambda_s P_s \Delta z}{\Delta r}, \qquad d'_P = \frac{A\Delta z}{\Delta t}\rho c_p$$

$$a_P = a_W + a_E + a_N + a_S + d'_P, \qquad d_P = d'_P T^o_{\text{wall},i,j}$$

The coefficients mentioned above are applicable for $2 \leqslant i \leqslant n_z - 1$ and $2 \leqslant j \leqslant n_r - 1$; for the nodes in the frontier the following considerations have been applied:

- For $j = 1$, forced convection is considered in the south face. Tube wall thermal conductivity in east and west faces and insulation thermal conductivity in north face are evaluated at the mean temperature between the nodes that separate them.
- For $j = n_r$, natural convection with the ambient (using the correlation developed by Churchill and Chu [15]) and conduction through the adjacent layer of insulation of thickness equal to $\Delta r/2$ are considered. Thermal conductivity values are evaluated at the node temperatures.
- For $i = 1$ and $i = n_z$, appropriate coefficients are used to take into account the axial heat conduction or temperature boundary conditions.

6. Numerical algorithm

At each time step solution process is carried out on the basis of a global algorithm that solves in a segregated manner the flow inside the inner tube, the flow inside the inner and outer annulus and the heat conduction in the inner and intermediate tubes and the outermost tube with insulation. The coupling between the six main subroutines has been performed iteratively at each time step following the procedure described below (see Fig. 4):

- *For fluid flow inside the inner tube*, the governing equations are solved considering the tube wall temperature distribution as boundary condition, evaluating the convective heat transfer in each CV.
- *For fluid flow inside the inner annulus*, the same process (as above) is carried out considering both wall temperatures (inner and intermediate tube wall).

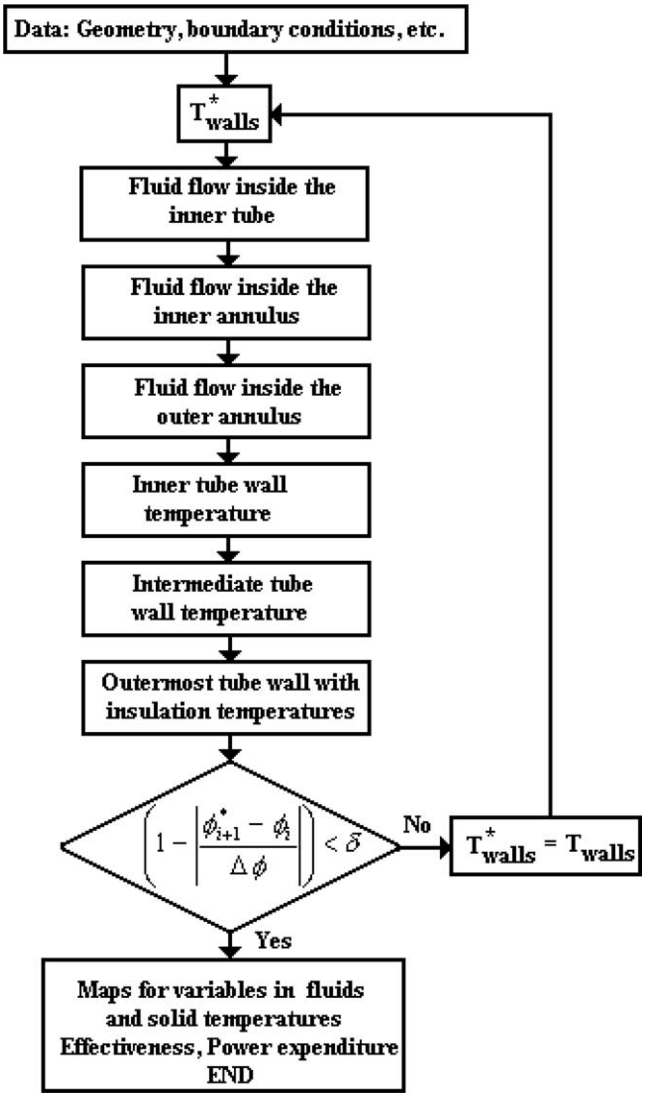

Fig. 4. Numerical algorithm flow diagram.

- *For fluid flow inside the outer annulus*, the same process (as above) is carried out considering both wall temperatures (intermediate tube wall and outermost tube wall).
- *In the inner tube wall*, the temperature distribution is re-calculated using the fluid flow temperature and convective heat transfer coefficients evaluated with the energy equation in the fluid flow inside the inner tube and the inner annulus.
- *In the intermediate tube wall*, the temperature distribution is re-calculated using the fluid flow temperature and convective heat transfer coefficients evaluated with the energy equation in the fluid flow inside the inner and outer annulus.
- *In the outermost tube with insulation*, the temperature distribution is re-calculated using fluid flow temperature and convective heat transfer coefficients evaluated with the energy equation in the outer annulus and the natural convection heat transfer coefficient evaluated for the external ambient according to Churchill and Chu [15].

It is assumed that the streams in the inner tube and the outer annulus are fed by the same pumping source which implies that the pressure drop at the inner tube and at outer annulus should be equal [3]. For this reason, the mass flow in each stream (inner tube and outer annulus) is iteratively evaluated by a Newton–Raphson algorithm in such a way that the pressure drop is the same, and the outlet pressure is also iteratively evaluated by a Newton–Raphson algorithm until the imbalance of the global mass conservation equation between the two streams is verified.

The governing discretized equations corresponding to a steady state situation are the same equations (5)–(7), (11), (12) without considering the temporal derivative terms. This situation can be solved using a pseudo-transient calculation with a guessed initial condition (for example, fluids a rest and uniform temperature in the whole domain). In transient situations, the initial conditions must be completely specified (i.e., the complete distribution of the variables in the whole domain). Sometimes these initial conditions are obtained from a steady state solution.

The global convergence is reached when between two consecutive loops of the six main subroutines is verified by Eq. (10) for all the CVs in the domain.

7. Numerical results

Results obtained with the numerical simulation developed are presented. Firstly, numerical result for the solids is compared with the analytical solution of a single case in order to verify this subroutine. Finally, different numerical results for triple concentric-tube heat exchanger are compared with data obtained from the technical literature, and the operational performance with counter and parallel flow arrangement are illustrated.

7.1. Comparison of numerical results with analytical solution

7.1.1. Comparison with an analytical solution for axial conduction in a tube

The code has been verified for the case of a single tube in steady state conditions. Extremes are considered isothermal. The internal and external fluids have different uniform temperatures with known uniform heat transfer coefficients.

The analytical solution (based on the standard theory of heat transfer for fin surfaces with constant sectional area) is generated for the axial condition in tubes as follows [16]:

$$T_{\text{wall},z} = C_1 e^{mz} + C_2 e^{-mz} + \overline{T} \tag{13}$$

where,

$$C_2 = \frac{\Phi_2 - \Phi_1 e^{mL}}{e^{-mL} - e^{mL}}, \qquad C_1 = \Phi_1 - C_2$$

$$\Phi_1 = \left(T_{\text{extreme},w} - \overline{T}\right), \qquad \Phi_2 = \left(T_{\text{extreme},e} - \overline{T}\right)$$

$$\overline{T} = \frac{\alpha_{\text{fluid,ext}} P_{\text{ext}} T_{\text{fluid,ext}} + \alpha_{\text{fluid,int}} P_{\text{int}} T_{\text{fluid,int}}}{\alpha_{\text{fluid,ext}} P_{\text{ext}} + \alpha_{\text{fluid,int}} P_{\text{int}}}$$

$$m^2 = \frac{\alpha_{\text{fluid,ext}} P_{\text{ext}} + \alpha_{\text{fluid,int}} P_{\text{int}}}{\lambda_{\text{wall}} A}$$

The comparison between numerical and analytical solutions has been made for the following case: $T_{\text{extreme},w} = 30\,^{\circ}\text{C}$, $T_{\text{extreme},e} = 51\,^{\circ}\text{C}$, $T_{\text{fluid,ext}} = 45\,^{\circ}\text{C}$, $T_{\text{fluid,int}} = 28.5\,^{\circ}\text{C}$, $\alpha_{\text{fluid,ext}} = 20\ \text{W}\cdot\text{m}^{-2}\cdot\text{K}^{-1}$, $\alpha_{\text{fluid,int}} = 40\ \text{W}\cdot\text{m}^{-2}\cdot\text{K}^{-1}$, $D_{\text{int}} = 0.0079$ m, $D_{\text{ext}} = 0.0095$ m, $L = 1.0$ m, $\lambda_{\text{wall}} = 400\ \text{W}\cdot\text{m}^{-1}\cdot\text{K}^{-1}$ (the conductivity is approximately of copper tubes).

In this case, the maximum error in a CV is lower that 0.06% for grids with more than 40 CVs. Fig. 5 shows the comparison between analytical and numerical results for the case of 40 CVs. An excellent degree of correlation can be

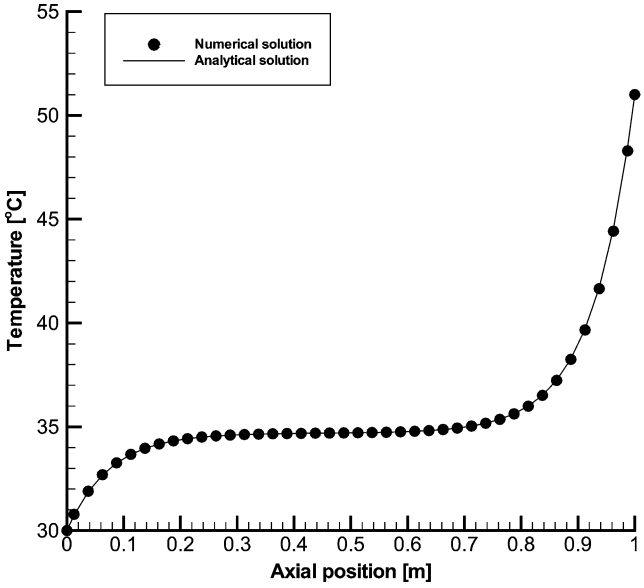

Fig. 5. Comparison between analytical and numerical solution using 40 grid nodes.

observed in the numerical solution with a reasonable number of CVs. The sigmoidal trend of this curve is due to that the heat transfer by convection is higher than the heat transfer by conduction therefore only near the extremes the heat transfer by conduction is appreciable and the temperature tends to the extremes temperatures. If the heat transfer by conduction will be much higher than the heat transfer by convection then the profile of this curve should be a line between the two extremes temperatures.

7.2. Comparison of numerical results of triple-tube heat exchangers with technical literature data

In these analyses, the mass flux inside the inner tube and the outer annulus are determined considering that both streams have the same pressure drop along the heat exchanger as mentioned in the section for *numerical algorithm*.

Once the mass flow rate and the temperature distribution are determined, the heat exchanger effectiveness ε is calculated as a performance parameter using the next definition [3]:

$$\varepsilon \equiv \frac{\dot{Q}}{\dot{Q}_{\max}} \equiv \frac{\|\dot{m}_2(h_{2,\text{out}} - h_{2,\text{in}})\|}{\|(\dot{m}c_p)_{\min}(T_{2,\text{in}} - T_{1,\text{in}})\|} \tag{14}$$

The total friction power expenditure P_T is used as another performance parameter, which is calculated from [3]:

$$P_T = \frac{\dot{m}_1 \Delta p_1}{\bar{\rho}_1} + \frac{\dot{m}_2 \Delta p_2}{\bar{\rho}_2} + \frac{\dot{m}_3 \Delta p_3}{\bar{\rho}_3} \tag{15}$$

Where subscript 1, 2 and 3 indicate the flow inside the inner tube, the inner annulus and the outer annulus respectively.

All the numerical results presented in this paper have been obtained using an appropriate number of CVs to get grid-independent solutions.

7.2.1. Comparison with the theoretical analysis by Ünal [3]

In this section, different cases corresponding to a counter-flow triple concentric-tube heat exchanger are compared with the theoretical values obtained by Ünal [3].

For all the cases (see Fig. 3): $L = 30$ m, $r_5 = 80 \times 10^{-3}$ m, $r_7 = 87 \times 10^{-3}$ m, $(r_2 - r_1) = 1 \times 10^{-3}$ m (thickness of the inner tube), $(r_4 - r_3)$ and $(r_6 - r_5) = 2 \times 10^{-3}$ m (thickness of the intermediate and outermost tube respectively), $\theta = 0$ and $\xi = 1.5 \times 10^{-6}$ m for all the surfaces. Tubes are of stainless steel and the insulation of armaflex. The ambient temperature has been fixed in 25 °C. The numerical parameters are: $\delta = 10^{-6}$, $\Delta z = 0.1$ m and $n_r = 5$. The empirical correlations used in this case are the same as mentioned in the section for *evaluation of empirical coefficients*.

A liquid food product with a constant thermophysical properties of $\rho_2 = 1020$ kg·m^{-3}, $c_{p2} = 4000$ J·kg^{-1}·K^{-1}, $\mu_2 = 1.5 \times 10^{-3}$ Pa·s, $\lambda_2 = 0.5$ W·m^{-1}·K^{-1} and an inlet temperature of 80 °C has been considered as the hot fluid. Water at $T_1 = T_3 = 15$ °C, $p_1 = p_3 = 1$ bar and $\dot{m}_{13} = \dot{m}_1 + \dot{m}_3 = 10000$ kg·h^{-1} has been considered as the cold fluid entering the heat exchanger (variable thermophysical properties according to REFPROP v.7.0 [8] has been taken into account for water). The hot fluid is considered to be flowing in counter-flow direction in the inner annulus and for the case of $r_1 = r_2 = 0$ m (double concentric-tube heat exchanger) it is considered to be flowing inside the inner tube.

The analyses are carried out by taking a fixed value of the intermediate tube radius, r_3, at a time and varying the size of the inner tube, r_1, between $r_1 = 10 \times 10^{-3}$ m and $r_1 = (r_3 - \Delta r_1)$ m with $\Delta r_1 = 5 \times 10^{-3}$ m intervals. Five values of r_3 ($r_3 = 30$, 40, 50, 60 and 70×10^{-3} m) are considered. Case studies have been carried out for three different mass flow rates of the hot fluid ($\dot{m}_2 = 2000$, 3000 and 5000 kg·h^{-1}).

Differences between the results obtained with the steady state model by Ünal [3], and the formulation model presented in this paper are principally due to the following reasons: the correlations used for the heat transfer coefficient and the friction factor are different between both works (and also, the transition criterion between laminar and turbulent regimes, in this work the critical Reynolds number is 2000 and in the Ünal's work is 2300); the flow through the inner tube and the outer annulus is evaluated by Ünal [3] considering frictional drops only (neglecting local pressure drops). In this work, the mass flow in each stream (inner tube and outer annulus) is iteratively evaluated by a Newton–Raphson algorithm in such a way that the pressure drop is the same, and the outlet pressure is also iteratively evaluated by a Newton–Raphson algorithm until the imbalance of the global mass conservation equation between the two streams is verified; Ünal's [3] work does not take into account the thickness of tubes and it does not consider the thermal resistance and heat transfer through tube wall. Also the cross sectional areas of flow are different because Ünal's [3] does not take into account the thickness of tubes; Ünal [3] considers thermophysical properties of water to be constant which, in the analyses, results in constant heat transfer coefficients along the flow instead of a variable one. In spite of the differences mentioned above, both models give similar tendencies for the analyses cases (as it is demonstrated later) with all the three flows presented in the triple concentric-tube heat exchanger in a turbulent regime.

Fig. 6(a), (b) show as Ünal [3] mentioned and the model confirms: "It is clear that larger effectiveness are achieved for small values of r_3, especifically for $r_3 = 40 \times 10^{-3}$ m and 50×10^{-3} m (in the model here presented also larger effectiveness are obtained for $r_3 = 60 \times 10^{-3}$ m)". With a double tube heat exchanger of same length and outer tube radius ($L = 30$ m and $r_5 = 80 \times 10^{-3}$ m, considering $r_1 = r_2 = 0$ m) would yield a maximun effectiveness of $\varepsilon = 0.528$ at an inner diameter of $r_3 = 50 \times 10^{-3}$ m; it is apparent from Fig. 6(a) that adding a third tube with a radius of $r_1 = 30 \times 10^{-3}$ m, for example, would increase the effectiveness to a value of $\varepsilon = 0.843$ which may be translated into more than

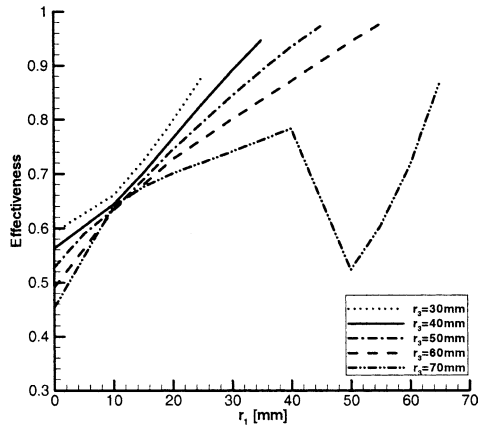

(a)

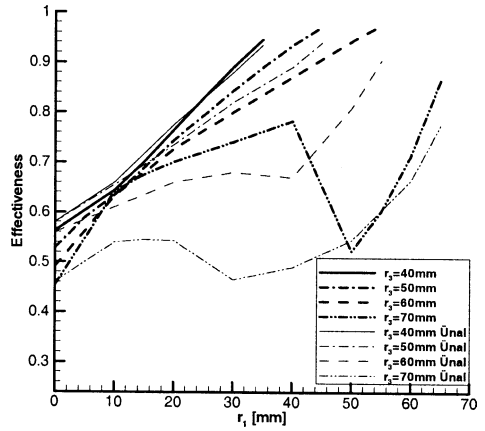

(b)

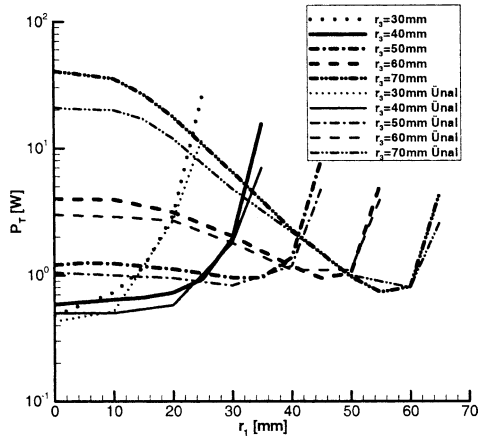

(c)

Fig. 6. Variation of (a) effectiveness and comparison with results obtained by Ünal [3] of (b) effectiveness and (c) total frictional power expenditure with the inner and intermediate tube radius, for a triple tube heat exchanger when $\dot{m}_2 = 2000$ kg·h^{-1}.

30% increase in the exchanger duty (heat transfer rate). Even a larger value of $\varepsilon = 0.972$ could be obtained if the inner tube radius is increased to $r_1 = 45 \times 10^{-3}$ m for the expense of $P_T = 7.946$ W instead of the value of $P_T = 0.956$ W occurring at $r_1 = 30 \times 10^{-3}$ m (see Fig. 6(c)). The model estimated a better operational point for $r_3 = 60 \times 10^{-3}$ m

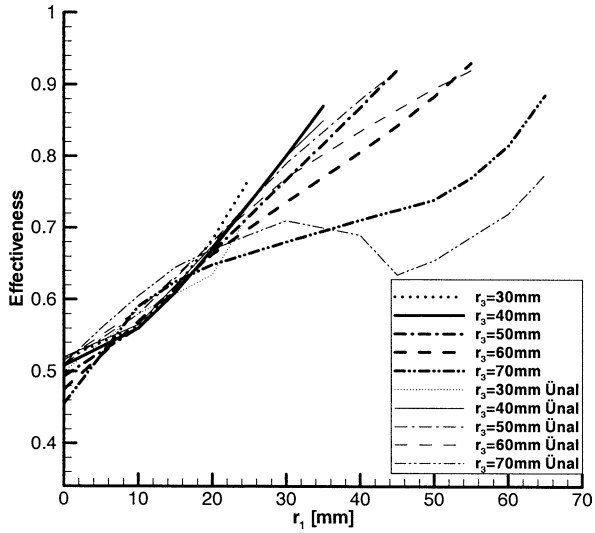

(a)

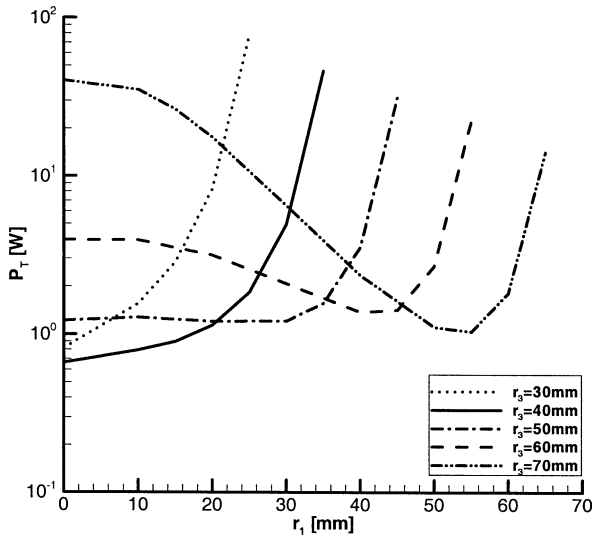

(b)

Fig. 7. Variation and comparison with results obtained by Ünal [3] of (a) effectiveness, (b) total frictional power expenditure with the inner and intermediate tube radius, for a triple tube heat exchanger when $\dot{m}_2 = 3000$ kg·h^{-1}.

when $r_1 = 50 \times 10^{-3}$ m, with the performance parameters of $\varepsilon = 0.943$ and $P_T = 1.038$ W. The exchanger effectiveness owes its higher values for $30 \times 10^{-3} \leqslant r_3 \leqslant 60 \times 10^{-3}$ m to turbulent fluid flows in all the three streams.

Fig. 6(c) shows as Ünal [3] mentioned and the model confirms: "For small values of r_3 ($r_3 \leqslant 50 \times 10^{-3}$ m), P_T is quite low at the beginning. For larger values of r_3 ($r_3 \geqslant 60 \times 10^{-3}$ m) relatively high total frictional power expenditures are obtained at small r_1".

Fig. 6(a)–(c) show that relative sizes of the tubes (tube radius) that form the heat exchanger play a very important role on the exchanger performance.

Figs. 7(a), (b) and 8(a), (b) show that the most convenient operational exchanger parameters are limited within the range of $r_3 = 60 \times 10^{-3}$ m and $r_1 = 40 \times 10^{-3}$ m to

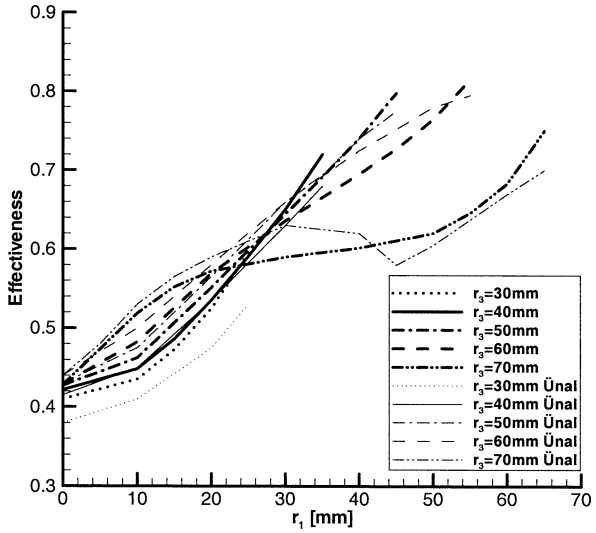

(a)

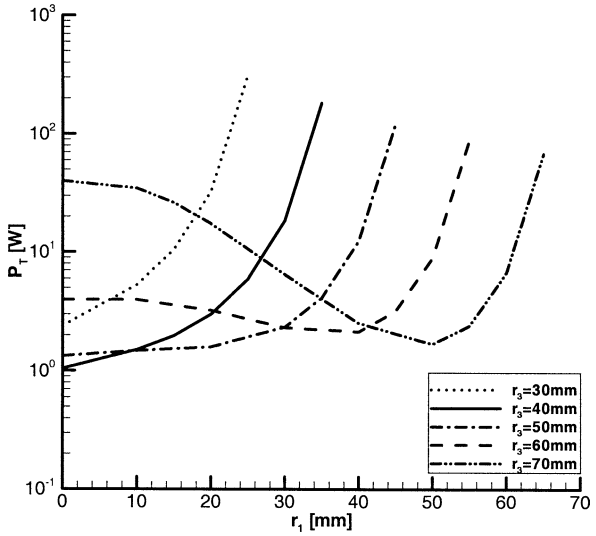

(b)

Fig. 8. Variation and comparison with results obtained by Ünal [3] of (a) effectiveness, (b) total frictional power expenditure with the inner and intermediate tube radius, for a triple tube heat exchanger when $\dot{m}_2 = 5000$ kg·h^{-1}.

50×10^{-3} m for $\dot{m}_2 = 3000$ kg·h^{-1} and $r_3 = 60 \times 10^{-3}$ m and $r_1 = 35 \times 10^{-3}$ m to 45×10^{-3} m for $\dot{m}_2 = 5000$ kg·h^{-1}.

Laminar flow conditions where found in some parts of the heat exchanger in the following cases: in the flow in the inner tube for $r_1 = 10 \times 10^{-3}$ m and $r_3 = 30 \times 10^{-3}$ m to 40×10^{-3} m; for the flow in the outer annulus for $r_1 > 50 \times 10^{-3}$ m and $r_3 = 70 \times 10^{-3}$ m. For both situations, the laminar regime produce lower heat transfer coefficients but it does not affect the numerical results significantly because the mass flow through these tubes for these cases is very low compared with the flow in the outer annulus or in the inner tube, respectively; for the flow in the inner annulus for $r_1 > 50 \times 10^{-3}$ m and $r_3 = 70 \times 10^{-3}$ m and $\dot{m}_2 = 2000$ kg·h^{-1}. Laminar regime in this case affects a lot the numerical results as it is shown in Fig. 6(a); the discontinuity in this dashed-dotted-dotted line is due to a large change in the heat transfer coefficient between laminar and turbulent flows.

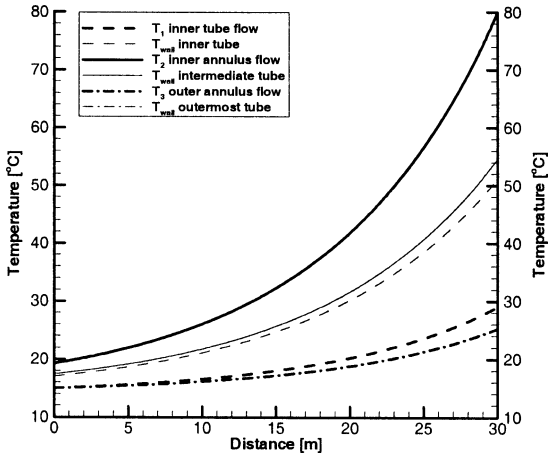

(a)

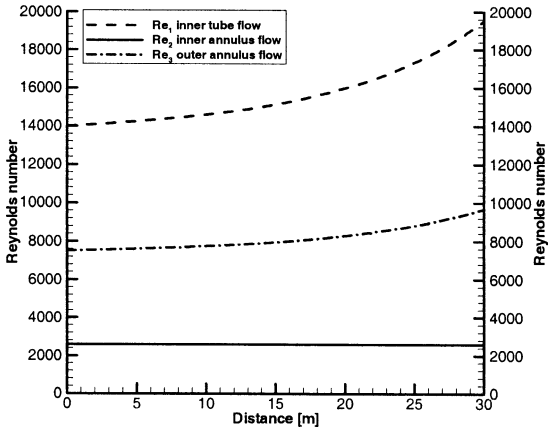

(b)

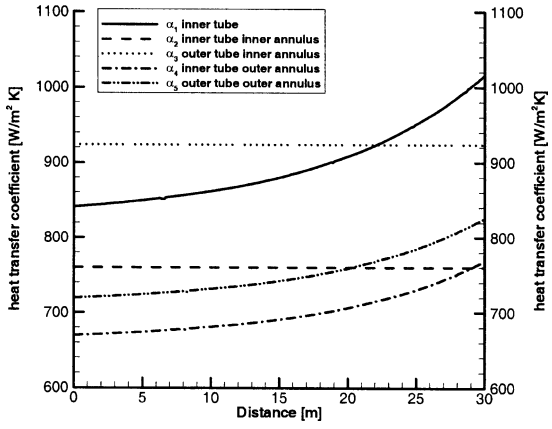

(c)

Fig. 9. Numerical (a) temperatures, (b) Reynolds numbers and (c) heat transfer coefficients distribution for a counter flow triple tube heat exchanger ($r_1 = 40 \times 10^{-3}$ m, $r_3 = 50 \times 10^{-3}$ m and $\dot{m}_2 = 2000$ kg·h^{-1}).

Fig. 9(a)–(c) illustrates the temperatures, Reynolds numbers and heat transfer coefficients along a counter flow triple-tube heat exchanger with $r_1 = 40 \times 10^{-3}$ m, $r_3 = 50 \times 10^{-3}$ m and $\dot{m}_2 = 2000$ kg·h^{-1}. Fig. 9(a) shows the simulation flows and tube wall temperatures along the heat ex-

changer; the flow temperatures between the fluid in the inner annulus and the water in the inner tube and outer annulus increases with the distance due to the counter flow arrangement. Fig. 9(b) shows the Reynolds number profiles. It is clear in this figure that considering variable thermophysical properties in the water, the Reynolds number has important changes along the heat exchanger (for example, in Fig. 9(b), in the inner tube and the outer annulus the Reynolds number ranges from 14000 to 19540 and from 7520 to 9660 respectively; these changes are due to that the dynamic viscosity in the water changes with temperature, for example, in the inner tube considering an atmospheric pressure, $\mu = 1.139 \times 10^{-3}$ Pa·s at 15 °C and $\mu = 8.157 \times 10^{-4}$ Pa·s at 29 °C). This produces important variations in the heat transfer coefficients (Fig. 9(c)). Due to this the heat transfer between different flows and the effectiveness in the heat exchanger can change significantly compared with cases considering constant thermophysical properties (as in liquid food in the inner annulus, where the Reynolds number and the heat transfer coefficient remain constant along the length of the heat exchanger).

7.2.2. Comparison between a counter-flow and a parallel flow triple concentric-tube heat exchanger

The same case presented above with the inner annulus mass flow rate of 2000 kg·h^{-1} ($\dot{m}_2$) and $r_3 = 40 \times 10^{-3}$ m to 60×10^{-3} m is now evaluated considering that heat exchanger works in parallel arrangement. The numerical results obtained for these cases are compared with the results obtained for the counter-flow ones.

Fig. 10(a) shows that the differences between both flow arrangements are relatively small for small values of r_1, but they increase with increases in r_1 (this is due to that with small values of r_1 the mass flow rate and the heat transfer area through the flow inside the inner tube is too small and the heat transfer of this fluid to the fluid in the inner annulus is also small, with increases in r_1 these values are higher and due to the effectiveness of a counter flow arrangement in the inner tube is higher than in a parallel one, also the difference in the global effectiveness in the heat exchanger between both arrangement increases). Comparing both configurations (parallel and counter-flow arrangement) for their better operation points ($r_3 = 60 \times 10^{-3}$ m when $r_1 = 50 \times 10^{-3}$ m, with the performance parameters of $\varepsilon = 0.943$ for counter-flow arrangement and $\varepsilon = 0.811$ for parallel arrangement), the effectiveness would increase by more than 12% using a counter-flow arrangement.

Fig. 10(b) shows the temperature distribution along the heat exchanger for both arrangements (the case is the same of Fig. 9(a), $r_1 = 40 \times 10^{-3}$ m, $r_3 = 50 \times 10^{-3}$ m and $\dot{m}_2 = 2000$ kg·h^{-1}), for the flow in the inner tube and in the inner and outer annulus. The outlet temperature in the inner annulus (T_2, liquid food) in the counter flow arrangement is about 7 °C lower than in the parallel one (this is due to the effectiveness in the counter flow arrangement is higher and the heat transfer rate between the water and

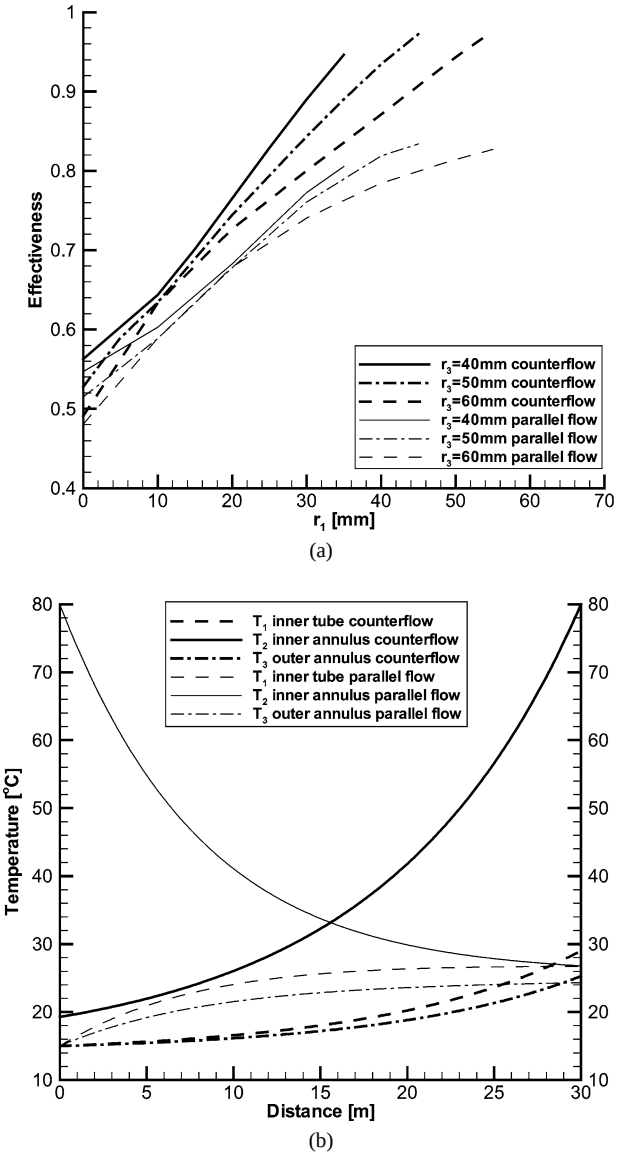

Fig. 10. (a) Variation of effectiveness and (b) temperatures distribution along the heat exchanger with a counter flow and parallel flow arrangement.

liquid food is better than with a parallel flow arrangement). The temperature difference between the liquid food in the inner annulus and water in the inner tube and outer annulus increases with the distance from the inlet of the heat exchanger (inlet is represented by a distance equal to 0 m in Fig. 10(b)) for counter flow arrangement, while it decreases for parallel flow.

7.2.3. Comparison with a simplified model

The case (same as Fig. 9(a), $r_1 = 40 \times 10^{-3}$ m, $r_3 = 50 \times 10^{-3}$ m and $\dot{m}_2 = 2000$ kg·h^{-1}) has been evaluated with a simplified model that considers thermophysical properties of water to be constant ($\rho = 999$ kg·m^{-3}, $c_p = 4189$ J·kg^{-1}·K^{-1}, $\mu = 1.14 \times 10^{-3}$ Pa·s, $\lambda = 0.59$ W·m^{-1}·K^{-1}) and without considering the thickness of tubes and with it, it does not consider the thermal resistance and heat transfer through tube wall.

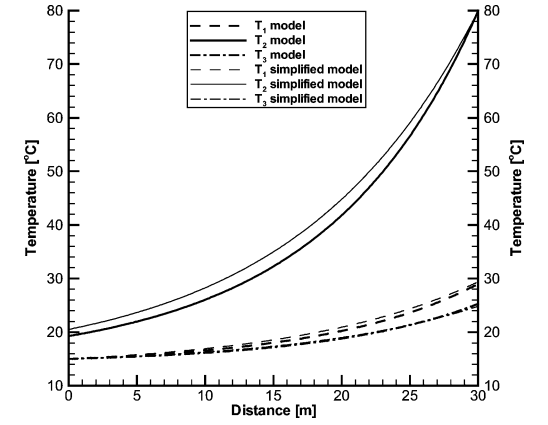

(a)

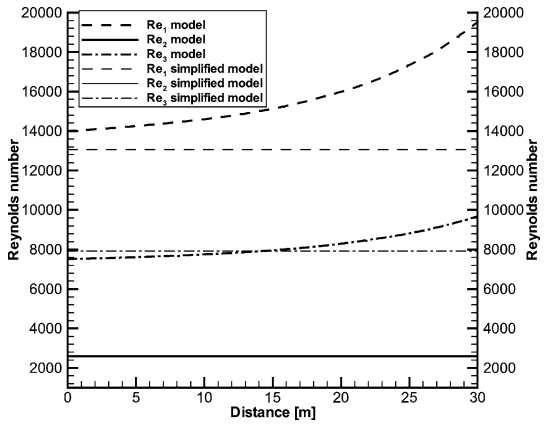

(b)

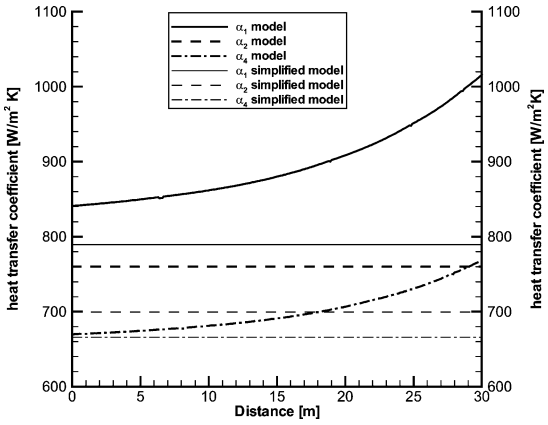

(c)

Fig. 11. Numerical (a) temperatures, (b) Reynolds number and (c) heat transfer coefficients distribution along the heat exchanger with the model and a simplified one.

Fig. 11(a)–(c) illustrates the temperatures, Reynolds numbers and heat transfer coefficients between the simplified model and the complete one here developed. Fig. 11(a) shows the variation in simulation flows and tube wall temperatures along the heat exchanger for both models; Fig. 11(b) shows the Reynolds number profiles. It is clear in this figure that considering variable thermophysical properties in the water, the Reynolds number has important changes along the heat exchanger. This produces important variations in the heat transfer coefficients (Fig. 11(c)). Due to this the heat transfer between different flows and the effectiveness obtained in the heat exchanger can change significantly using a simplified model.

The performance parameters for this simplified model are $\varepsilon = 0.915$ and $P_T = 1.121$ W against $\varepsilon = 0.934$ and $P_T = 1.375$ W, obtained with the model considering thickness of tubes, heat transfer through them and variable thermophysical properties of water. A relative discrepancy of 2.1% in the effectiveness and 18.5% in the power expenditure (P_T) has been obtained between both models. If the same case is evaluated changing the length of the heat exchanger to 10 m instead of 30 m, the effectiveness calculated with the simplified model is 0.585 against 0.621 obtained with the complete model. Therefore a relative discrepancy of 5.8% has been obtained.

According to the results obtained in this section, the difference between the model here presented and a simplified one will depend of the geometry, material, fluids and working conditions used (for example, in this case, if the thickness of the tubes is greater, the tubes materials present lower thermal conductivity than stainless steel and the thermophysical properties of the fluids have more important changes with the temperature, the discrepancies obtained between a simplified and a complete model could be much more important).

Moreover, the complete model here presented considers more realistic situations, such as transient effects, heat conduction within the tube walls, temperature dependent fluid properties and the possibility of two-phase flow conditions. Analytical approaches (Zuritz [1], Ünal [2–4]) cannot consider these possibilities.

Other considerations. As the mass flow in two streams (inner tube and outer annulus) is iteratively evaluated by a Newton–Raphson algorithm in such a way that the pressure drop is the same, and the outlet pressure is also iteratively evaluated by a Newton–Raphson algorithm until the imbalance of the global mass conservation equation between the two streams is verified, depending on the real triple concentric-tube heat exchanger geometry and the number and type of singularities (for example, inlet and outlet sections, see Fig. 12(a), and elbows, see Fig. 12(b)), the pressure drop through these singularities in the heat exchanger could greatly affect the flow through both streams (inner tube and outer annulus) due way the flow is evaluated in each one.

For this reason, information about the specific construction and final installation of each triple concentric-tube heat exchanger given by the manufacturer is needed in order to introduce in the model the pressure drop and heat transfer in these singularities and obtain more accurate results for predicting their thermal and fluid-dynamic behaviour comparing it with a real system. In this way, the model here presented can be an excellent tool to optimise the efficiency

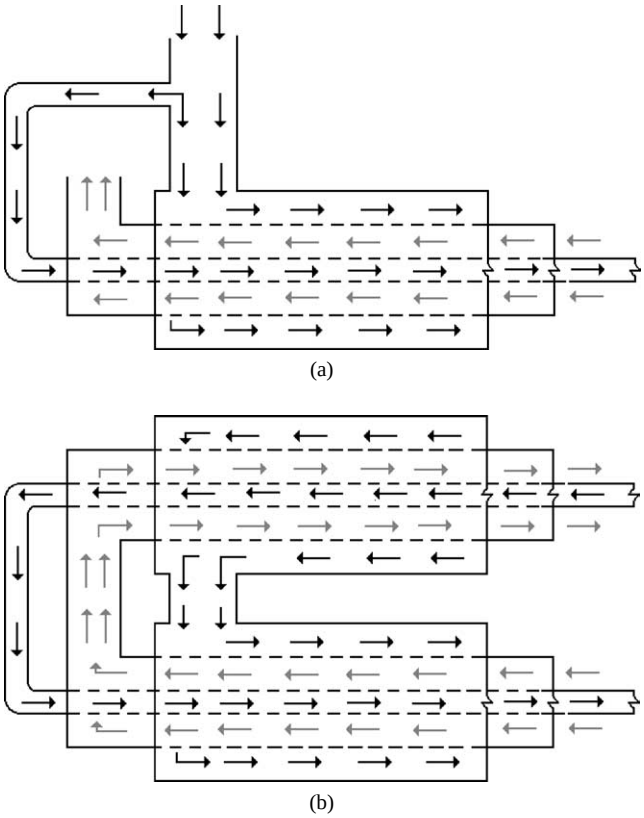

Fig. 12. Singularities in triple concentric-tube heat exchanger: (a) inlet and outlet sections and (b) elbows (if they exist).

of triple tube heat exchangers, and consequently the energy consumption.

8. Concluding remarks

A numerical model for analyzing the behaviour of triple concentric-tube heat exchangers has been developed by means of a transient one-dimensional analysis of the fluid flow governing equations and the heat conduction in solids. The empirical coefficients used in the model to evaluate the shear stress and heat flux have been chosen after a comparison of different options proposed in the technical literature.

The simulation has been implemented on the basis of an implicit step by step numerical scheme for the fluid flow inside the inner tube and annulus, and an implicit central difference numerical scheme in the solids. The six zones that form the triple-tube heat exchanger are solved iteratively in a segregated way until convergence is reached. The model considers heat transfer in solids, local thermophysical properties and local empirical coefficients in each CV.

The discretized governing equations allowed extension of this numerical model to cases where evaporation or condensation appeared inside this type of heat exchanger, considering adequate empirical correlations for these zones and also with the knowledge of the thermophysical properties of the fluid or fluids for these conditions.

The model presented considers realistic situations, such as transient effects, heat conduction within the tube walls and insulation, temperature dependent fluid properties and the possibility of two-phase flow conditions. Analytical approaches cannot consider these possibilities.

The models for solid walls and insulation developed have been validated with analytical solution of heat conduction. In general, the flexibility and generality of the detailed simulation model is demonstrated in this paper by comparison with different cases.

The model developed can be an excellent tool to optimise the efficiency of triple concentric-tube heat exchangers, and consequently the energy consumption.

References

[1] C. Zuritz, On the design of triple concentric-tube heat exchangers, J. Food Process Engrg. 12 (1990) 113–130.
[2] A. Ünal, Theoretical analysis of triple concentric-tube heat exchanger. Part 1: Mathematical modelling, Internat. Comm. Heat Mass Transfer 25 (7) (1998) 949–958.
[3] A. Ünal, Theoretical analysis of triple concentric-tube heat exchanger. Part 2: case studies, Internat. Comm. Heat Mass Transfer 28 (2) (2001) 243–256.
[4] A. Ünal, Effectiveness-NTU relations for triple concentric-tube heat exchangers, Internat. Comm. Heat Mass Transfer 30 (2) (2003) 261–272.
[5] F. Escanes, C.D. Pérez-Segarra, A. Oliva, Thermal and fluid-dynamic behaviour of double-pipe condensers and evaporators—a numerical study, Internat. J. Numer. Methods Heat Fluid Flow 5 (9) (1995) 781–795.
[6] O. García-Valladares, C.D. Pérez-Segarra, J. Rigola, A. Oliva, Detailed numerical simulation of condensers and evaporators using pure and mixed refrigerants, in: Proceedings of the 1998 International Compressor Eng. Conference at Purdue 2, Soedel, 1998, pp. 839–844.
[7] O. García-Valladares, C.D. Pérez-Segarra, A. Oliva, Numerical simulation of capillary tube expansion devices behaviour with pure and mixed refrigerants considering metastable region. Part I: Mathematical formulation and numerical model, Appl. Thermal Engrg. 22 (2) (2002) 173–182.
[8] REFPROP version 7.0, Reference Fluid Thermodynamic and Transport Properties, NIST Standard Reference Database 23, Lemmon E.W., McLinden M.O., Huber M.L., USA, 2002.
[9] G.F. Hewitt, Heat Exchanger Design Handbook 2002, Part 2: Fluid Mechanics and Heat Transfer, Begell House, New York, 2002, pp. 2.3.2–11.
[10] V. Gnielinski, New equations for heat and mass transfer in turbulent pipe and channel flow, Internat. Chem. Engrg. 16 (1976) 359–368.
[11] S. Lin, C.C. Kwok, R.Y. Li, Z.H. Chen, Z.Y. Chen, Local frictional pressure drop during vaporization of R-12 through capillary tubes, Internat. J. Multiphase Flow 17 (1) (1991) 95–102.
[12] M. Jakob, Heat Transfer, Wiley, New York, 1949, p. 552.
[13] H. Martin, Lecture on Heat Transfer II, Universität Karlsruhe, TH, 1990.
[14] S.V. Patankar, Numerical Heat Transfer and Fluid Flow, McGraw-Hill, New York, 1980.
[15] S.W. Churchill, H.H.S. Chu, Correlating equations for laminar and turbulent free Convection from a horizontal cylinder, Internat. J. Heat Mass Transfer 18 (9) (1975) 1049–1053.
[16] L.C. Thomas, Fundamentals of Heat Transfer, Prentice-Hall, Englewood Cliffs, NJ, 1980, pp. 81–83.